RESEARCH ARTICLE

INTERNATIONAL RESEARCH JOURNAL OF MULTIDISCIPLINARY TECHNOVATION

Asian Research Association

DOI: 10.54392/irjmt25412

Advanced Computer Vision Model for Lung Tumor Segmentation and Detection in Radiology and Histopathology Images

T.S. Sheeja [a,*], Arun Chokkalingam [a]

[a] Department of Biomedical Engineering, Vels Institute of Science, Technology & Advanced Studies (VISTAS), Chennai, India

* Corresponding Author Email: sheebio123@outlook.com

DOI: https://doi.org/10.54392/irjmt25412

Received: 11-04-2025; Revised: 19-06-2025; Accepted: 05-07-2025; Published: 20-07-2025

Abstract: For effective treatment scheme and initial diagnosis, it is important to segue and detect the lung tumors. Tumor variability, low contrast and overlapping tissue structure are some problems with traditional methods that make it challenging to accurately and detect it. So, a newly advanced computer vision model that uses a Binary Gennet Optimizer Tund Forward Neural Network (BGO-FFNN) method is used to sort tumors. The dataset contains anotate CT scan and histopathology slides that were taken from publicly available repository. Gabber filters are used in preprosauting to get rid of noise and strengthen the opposite, making it easier to see the edges of the tumor. Multi-scale edge-watthers' techniques work together for different tumor areas simultaneously. Local binary pattern (LBP) is used to achieve texture features, which are important to explain the difference between a variety of tumors. BGO is used to improve FFNN, and then classification performance is tested. The results showed that the suggested model improves with recall (94.48%), F1-score (97.21%), accuracy (95.14%), and accurate (99.71%). Results suggest that the proposed advanced computer vision model works better than standard people. This hybrid model creates a major difference on how well the tumor is found and classified. It is very likely to use in the clinic and helps radiologists and pathologists assess and diagnose the exact tumor. These enrichment improves clinical accuracy and streamlines the workflow in clinical settings. As technology is developed, further integration of artificial intelligence in medical imaging can lead to more significant progress in patient results.

Keywords: Lung tumor detection, Tumor segmentation, Feed Forward Neural Network (FFNN), Binary Gannet Optimizer (BGO), MATLAB simulation, Advanced Computer Vision Model

1. Introduction

According to a huge number of case-control analyses carried out in the early 2000s, lung cancer mortality was considerably decreased by a combined screening strategy that used sputum cytology and chest radiography [1]. For statistical image investigation with patients, including diagnosis, radiation, and response assessment, the detection as well as segmentation of anomalies in medical images are crucial [2]. Rapid detection and precise diagnosis of possibly malignant tumors would improve the effectiveness of therapy and lower the death rate from lung tumor. The lack of obvious signs until the lung tumor has spread is a major obstacle for early detection [3].

In many countries, lung tumors are the most dreadful diseases, and it is yet difficult to identify the disease in a timely manner with increased accuracy. Cancer experts use Computer Tomography (CT) images and blood test outcomes to evaluate the malignancy, which takes time and requires additional human labor [4].

CT scanning is regarded as a dependable visual modality, and doctors have been employing many visuals of cancer types for the past years. A number of clinical image processing methods were created to use CT images to diagnose lung cancer early or later, but enhancing the techniques' responsiveness and efficiency remains a serious problem [5]. Nanotechnology is also becoming increasingly more advantageous and is being used in numerous practical applications, like accurate diagnosis as well as minute tumor detection. The accuracy and preciseness of tumor identification, as well as the differentiation of both cancerous and benign tumors, are greatly enhanced by nanoscale imaging processes [6].

The identification of such cancers is especially important for research and therapy purposes. Through medical visualization techniques, namely machine learning (ML) as well as deep learning (DL), traditional strategies were exceeded [7]. Artificial intelligence (AI) in detecting radiography images is experiencing rapid growth. Its probable benefit to enhance diagnosis accuracy for tumor events is generally known, but the

efficiency and clarity have yet to be proved in the setting of present diagnostic techniques [8]. Absolute volume of tumor auto segmentation has the potential to reduce clinical demand and offer uniformity for irradiation treatment selection among physicians and organizations. Furthermore, auto segmentation can make it possible for imaging investigations like radiation to build and implement extensive analysis involving several thousand patients [9]. The cancerous tumors in the lung can also be identified by involving X-ray images for early detection and prevention. Radiology images are segmented using Otsu's approaches of thresholding, and feature vectors are produced from the histogram features and pixel counts. Different methods are employed to ascertain whether the tumors are malignant or benign [10].

The starting stage of the detection is currently the most effective strategy to increase the existence percentage of affected individuals. Typically, radiologists need a full study of CT images to detect lung tumors, which takes more time. It is essential to analyze lung tumor in neuroimaging modalities such as CT scans. Medical imaging modalities can be analyzed using image processing as a continuous diagnostic tool [11]. The process of dividing visual data into varied components is called as segmentations. Finding various features in a visual data is essential for monitoring the environment and more specifically, for healthcare. Though Magnetic Resonance Imaging (MRI) is highly effective in visualizing soft tissues, its application in lung tumor detection is complicated by respiratory movement. However, recent developments are enhancing its potential as a useful tool, especially for the staging and follow-up of lung cancer, providing a non-radiative option compared to CT in certain situations [12].

Even though a number of detection techniques, like combining chest scans and mucus cytology, have been shown to lower the death rate from lung cancer, more effective, precise and rapid detection techniques are indeed required. With mechanization and sophisticated processing of images, current methods like CT imaging and radiography can be made less demanding and time-consuming. Furthermore, although CT and MRI examinations are frequently used to identify lung cancer, these tests' responsiveness and effectiveness require considerable enhancement. Precision, pace, and uniformity problems yet plague the present segmentation procedures, especially when it comes to differentiating between malignant and benign tumors. To help radiologists, there is a chance to create increasingly complex segmentation and classification techniques. Although the increasing use of nanoparticles for health diagnosis, particularly for the detection of small tumors, shows promising results, it rather has to be improved upon and further incorporated into standard lung cancer diagnostic procedures [13]. Furthermore, there is currently a gap in the complete integration of AI-driven methodologies into clinical settings to improve cancer detection and treatment selection, even if ML and DL techniques have the potential to outperform conventional methods in medical imaging. Incorporating auto-segmentation technologies into medical processes and large-scale analysis requires more research, but research possess the capacity to handle massive amounts of patient data and offer consistency in treatment approaches. The lack of outward signs in the initial phases of lung tumor makes identification even more difficult, underscoring the need for better instruments to identify cancerous growths when they are still curable [14]. Additionally, although MRI is frequently used to diagnose various conditions, its utility in detecting lung cancer is less well-established than that of CT scans [15].

1.1 Key Contributions

- In data collection, the information contains annotated radiology (CT) scans and histopathology images obtained from public available repositories.
- Utilization of Gabor filters for preprocessing tends to improve clarity and lowers interference in the input medical images.
- Introducing a novel method, called BGO-FFNN for tumor classification, addressing shortcomings in conventional techniques.

2. Related Works

Several existing methods involved in lung tumor segmentation and classification were analyzed and are tabulated by comparing their objectives, methods, results and corresponding limitations. These are deliberated in Table 1.

Table 1. Comparison of Conventional Techniques engaging in Lung Tumor Segmentation and Classification

Reference	Objective	Method	Results	Limitation
[13]	To increase feature representation and address modality discrepancies	Images of PET as well as CT were separated using the MosNet approach	On 126 NSCLC PET-CT scans, MosNet demonstrated superior accuracy	Variations in malignancy size, image movement, and inhalation during radiology visuals.

[14]	The aim is to improve tumor segmentation	MSAM is used with PET scans.	The MSAM enhanced DSC by 7.6%	MSAM should extend to 3D tumor-positive slices, manual ground truth modifications, and single observer contouring.
[15]	Precise lung tumor segmentation and detection using highly improved methods.	Segmented lung cancerin radiology scans using a two-pathway deep supervision approach	Dice score of 0.675, F1-score of 0.682; on TCIA dataset.	Constrained by the multi-scale character of lung cancers that impact volumetric segmentation and the incapacity to efficiently learn tumor borders.
[16]	To effectively locate, segment, and classify lung tumors using a high degree of precision.	AGRes and U-Net, VGG-19 CNN were utilized for tumor classification; U-Net techniques assessed IOU.	CNN with Adam and VGG-19 optimized tumor diagnosis at improved accuracy, and AGRes U-Net obtained high accuracy.	Concentration on tumor segmentation and classification, with limited models that lacked refinement for a range of clinical scenarios.
[17]	Creating an automated system using scan images for lung tumor detection.	ExtRanFS framework for detection using NCCD dataset, which is also called IQ-OTH	Outperformed with improved F1-score, accuracy, and,sensitivity.	Utilizing a single dataset, ignoring variations in tumor features to the pre-trained VGG16 model limited the approach's utility.
[18]	Providing an overview for the detection of lung cancer.	JSRT, NLP, and 2D/3D CNNs.	Potential despite issues, going over traditional methods of lung cancer.	Underutilized transducer designs and insufficient for better precision and applicability.
[19]	Optimizing lung cancer detection and segmentation on CT scans.	DSC, statistical tests were used to assess a 3D U-Net.	DSC of 0.77, improved sensitivity, specificity, and a tumor segmentation time of 76.6 seconds.	Due to its dependence on typical chemotherapeutic data, the algorithm should be trained on a particular CT scan dataset, and could fail to generalize well.
[20]	To classify the lung tumor by giving several methods and achieve high precision	Hybrid WOA-APSO techniquewas used.	Algorithm achieved enhanced accuracy, sensitivity, and specificity rates.	Limited by the dependence of research on a particular radiology dataset, the hybrid WOA-APSO algorithm might have trouble with feature variability
[21]	Developed a design for quick and accurate lung cancer segmentation across all breathing phases.	Self-attention, motion region RCNN, and U-Net, techniques used.	VD of 0.50 as opposed to 0.99, 1.01, 0.92, outperformed and obtained DSC values of 0.86 and 0.90.	Due to its dependence on limited, high-quality 4D CT datasets and issues with tumor movement and structural changes
[22]	Developing an efficient CT image segmentation system for the diagnosis of tumor.	Three filters and GCPSO algorithm, as well as five optimization techniques were employed	Improving preprocessing and contrast, the GCPSO algorithm achieved the highest accuracy.	The use of only 20 specimen images, which may not adequately represent the range of lung CT scans, the results varied depending on the specific dataset

[23]	To overcome class imbalance, outperform other CNN architectures and accurately classify lung cancer from CT data.	The Lung-EffNet model, NCCD and other pre-trained CNN models.	Achieving high accuracy, and ROC score	A tiny dataset, no synthetic data generation, and a failure to investigate alternate topologies all hindered the model's performance.
[24]	To increase classification accuracy and enhance the identification of lung glands.	Preprocessing, CSAR algorithm is used to get higher accuracy.	Achieved optimized precision, recall, F1-score, accuracy.	Sensitivity of FCOM to initial centroids, and possible difficulties with complicated tumor forms.
[25]	Creating a precise framework for categorizing lung cancer nodules.	PCA Methodology is used.	Achieving improved accuracy.	Other medical imaging datasets, such as brain tumor identification, is its drawback.
[26]	To create a technique for diagnosing lung cancer with high accuracy and efficiency.	GCPSO algorithm for segmentation, and a graphical user interface for tumor categorization.	Obtained enhanced sensitivity, accuracy, precision, F1-score, and recall.	Lacked additional hyperparameter adjustment and was not extended to 3D images.
[27]	Created a technique to identify the problem automatically using radiology scans.	AlexNet-SVM model after modified U-Net.	High sensitivity, specificity, and precision accuracy.	The model was restricted to the LUNA16 dataset.
[28]	Evaluating lung cancer diagnosis techniques and proposing an effective tumor identification plan	Methods of classification and segmentation for the detection.	Accuracy in correctly detecting lung cancer	FCM could highlight the tumor but could not extract the tumor area effectively.

3. Methodology

The methods involved in this research include data collection consisting of annotated radiology images (CT scans) and histopathological slides. Preprocessing involves Gabor filters to reduce noise and improve the contrast of input images. MSEWS is used to segment tumors, for precise tumor zone delineation in spite of obstacles such as cell overlap and tumor variability [29]. LBP is used to extract texture information and to enhance classification accuracy, a novel method BGO-FFNN, which classifies tumors as normal and abnormal conditions. Figure 1 represents segmentation and classification of the BGO-FFNN model.

3.1 Data Collection

Radiological imaging data is gathered for classification and segmentation from Kaggle https://www.kaggle.com/datasets/dishantrathi20/ct-scan-images-for-lung-cancer. CT scan images are used for detection, which aids the diagnostic training ML models. The dataset consists of histopathological images collected to determine whether an image shown is benign, squamous cell carcinoma, or adenocarcinoma [30]. It is accumulated using https://www.kaggle.com/datasets/rm1000/lung-cancer-histopathological-images. Figure 2 signifies the sample images of histopathology and radiology images used for tumor detection.

3.2 Preprocessing

Preprocessing is the process of getting data ready and tidy in order to improve model performance by highlighting key characteristics, lowering noise, and increasing picture quality [31]. To provide precise tumor identification and classification in medical imaging, this phase is essential for enhancing the learning model's performance.

3.2.1 Gabor Filter

Gabor filters are frequently employed for texture classification-based applications such as reduction in noise and contrast enhancement of medical images. A sinusoidal plane wave modulated by a Gaussian envelope at a specific range and angle makes up a Gabor filter.

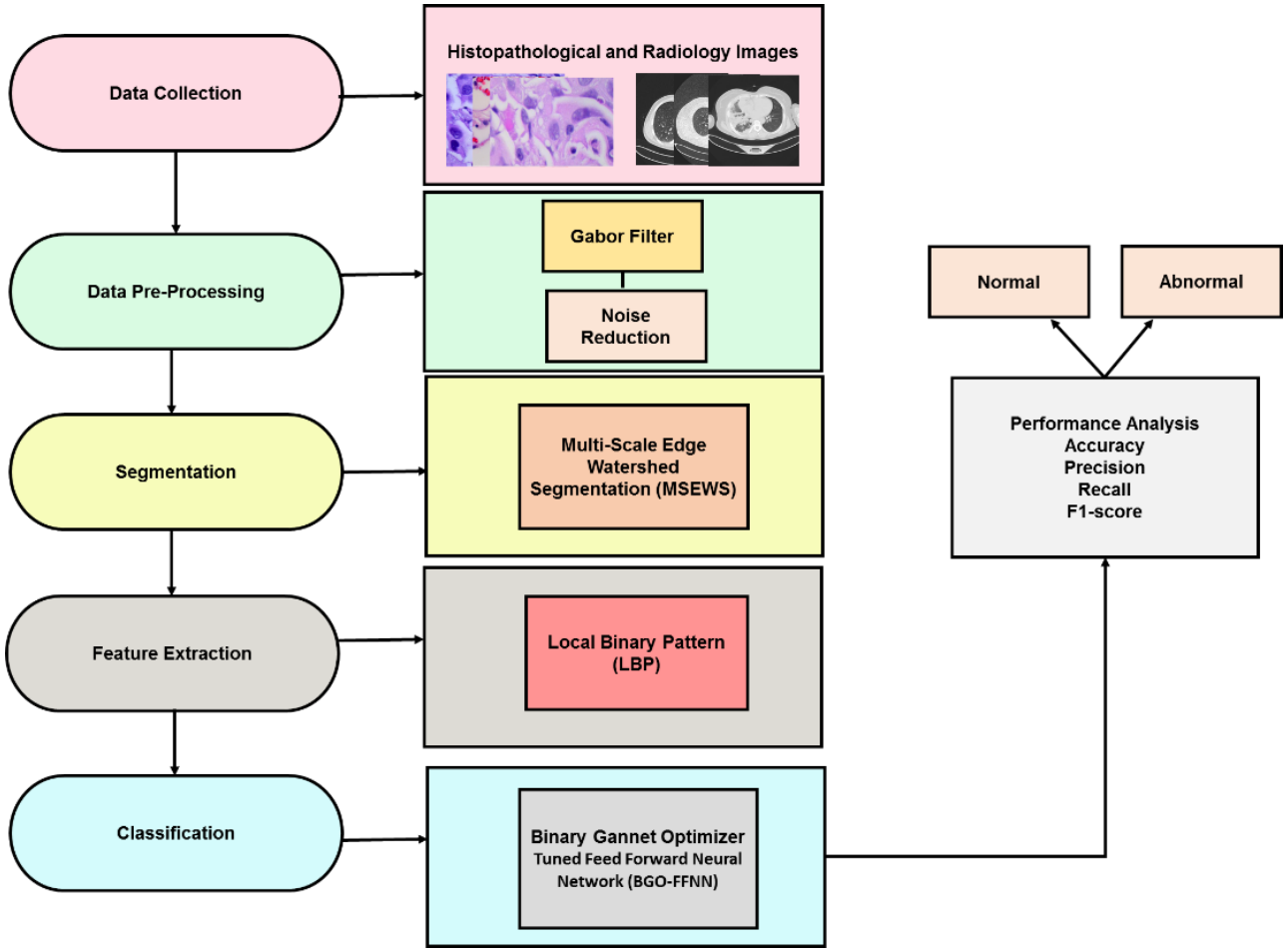

Figure 1. Overall Flow Diagram of Suggested Segmentation and Classification Model

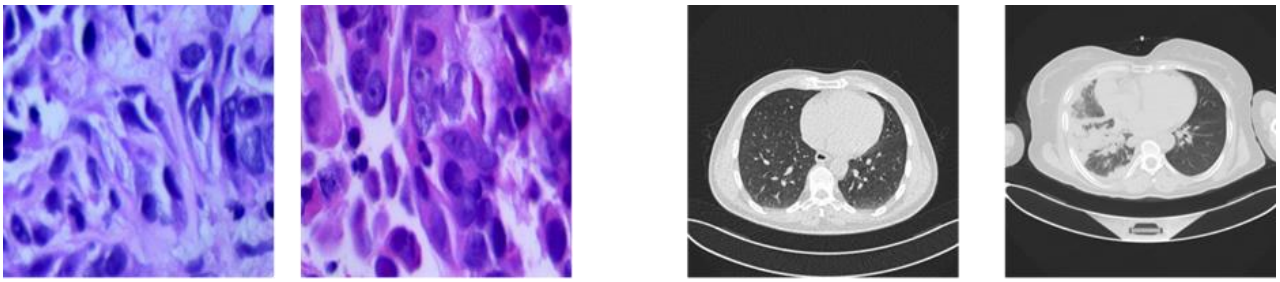

Figure 2. Sample Dataset Images (a) Histopathology and (b) Radiology Images

Convexity of images using a large amount of Gabor filters represents an image's Gabor filtering also defined by equations (1) and (2).

$$G_{\emptyset,\sigma}(W,Z) = J(W,Z) * \psi_{\theta,}\sigma(W,Z) \quad (1)$$

$$\int_{l=-\infty}^{+\infty}\int_{k=-\infty}^{+\infty} J(W,Z)\psi\theta \cdot \sigma(W-L\cdot Z-K) \quad (2)$$

Where, $J(\cdot)$ represents visual data, $\sigma(\cdot)$ symbolizes the direction of the Gabor filter. Here, θ and σ and $*$ is the operator for convolution and is possible to define a Gabor filter by using equation (3). The frequency-domain band pass filter is represented by equations (4) and (5).

$$\psi(V,U) = f\frac{-\pi^2}{e^2}\left(\gamma^2(v'-e)\right)2+\eta^2U^2) \quad (3)$$

$$u' = u\cos\theta + v\sin\theta \quad (4)$$

$$v' = -u\sin\theta + v\cos\theta \quad (5)$$

3.3 Tumor segmentation using Multi-Scale Edge-Watershed Segmentation (MSEWS)

Region-growing techniques, like watershed, are a common way to resolve image segmentation related issues. There are no restrictions to guarantee one marker per item or appropriate border placement in the Bayesian marker extraction approach, which uses a Naïve Bayes classifier. Therefore, a one-to-one correlation between markers and objects cannot be guaranteed. It can be mathematically defined in the equation (6).

$$K_{eroded} = K\theta A \quad (6)$$

The degradation of victualing label K is an appropriately selected structural component A. The results of G_{marker}, denoted as O_{marker}, is then represented in equation (7).

$$P_{marker}(j,i) = O[K_{eroded}(j,i)|e(j,i)] = g_{marker(e(j,i))} \quad (7)$$

Referring to the predictor learned in the usual reality and the outcome of the probability map is represented by K_{eroded} and g_{marker}, to emphasize the notational contrast. This is done in contrast with thresholding regions using larger values of O. The experimental findings will show that g_{marker} is unduly cautious and generates superior object markers.

Adjacent pixels can be differentiated to determine the intensity changes. Convolution of the filter to the image can be used to get the first order derivative. As a result, the object border might not be apparent. Thus, the MSEWS method successfully integrates erosion techniques with region-growing algorithms to enhance tumor segmentation, improving precision and clarity in medical imaging applications.

3.4 Feature Extraction using Local Binary Patterns (LBP)

Extracting the feature is an essential one to extract significant features for precise classification. Three matrices, such as object, edge, and background, typically appear throughout medical images of various types and can be identified by their feature qualities [32]. An image's local spatial pattern of pixel intensities is encoded by a texture descriptor called LBP. In terms of mathematics, each pixel's LBP is represented in equation (8).

$$LAQ(O,Q) = \sum_{O=0}^{0-1} e(h_o - h_f)\, 2^O \quad (8)$$

Where O indicates the entire number of pixels in radius that surround the central pixel. Additionally, the magnitude of the middle pixel is denoted by (h_o), whereas that of the neighboring pixels is denoted by h_f. If the radius of circulation is equal to one, then each central pixel in the (O,Q) image has eight associates in the LBP feature vector [33]. The LBP value is determined by evaluating the intensity of the central pixel in relation to its neighboring pixels, resulting in a binary pattern. These patterns are subsequently transformed into a numerical value that is utilized for classification. This aids in distinguishing structures such as lung tumors from the adjacent healthy tissue.

3.5 Lung Tumor Classification using Binary Gannet Optimizer Tuned Feed Forward Neural Network (BGO-FFNN)

To improve tumor classification performance, the BGO-FFNN uses the BGO's optimization capabilities to adjust an FFNN's parameters. It can optimize the FFNN with BGO, which addresses both local and global search capabilities and produces a more reliable and accurate model.

3.5.1 Feed Forward Neural Network (FFNN)

A FFNN comprises input, hidden, and output layers. Figure 3 shows the basic structure of an FFNN. The input layer accepts input data, hidden layers process information, and the output layer produces an output. The activation function ReLU is commonly used for tumor classification. The generic formulation shown in Equation (9) of the cross-entropy loss function used in the multi-class classification context is minimized through gradient descent.

$$QfKV = \begin{cases} w & w \geq 0 \\ 0 & w < 0 \end{cases} \quad (9)$$

$$k(\Theta) = -\frac{1}{m}\sum_{j=1}^{m}\sum_{i=1}^{r} z_i^{(j)}\, kmz_i^{(j)} \quad (10)$$

In equation (10), z is the input variable, $z_i^{(j)}$ is the tumor predicted label.

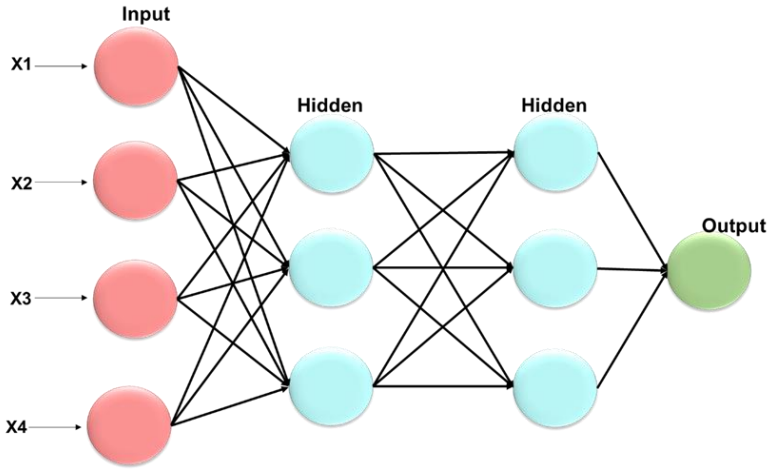

Figure 3. Architecture of Feed Forward Neural Network (FFNN)

3.5.2 Original Gannet Optimizer (GO) Algorithm

The GO is an evolution-based optimization method that employed to enhance the performance of tumor classification. In the design of the algorithm, inspiration was drawn from the behavior of gannets while feeding close to lakes and coastal waters: GO consists of two phases, namely exploitation and exploration, where the FFNN model is optimized for the purpose of tumor detection and classification.

3.5.2.1 Stage 1—Initialization

The gannets are considered to represent the initial population in this case, and it is started at random with value of limits as indicated by equation (11).

$$\mathrm{M}_{(\mathrm{o,r})} = E_1(VoA_r - KxA_r) + kxA \quad (11)$$

The position of o^{th} search tool of the r^{th} size was noted as $M_{(o,r)}$. The top bottom limits are represented as VoA and KxA. As seen in E_1, the random number falls between 0 and 1.

3.5.2.2 Stage 2—Exploration

In this step, the gannets search the water's surface for food. Once the prey has been located, it may change their diving techniques based in the water's depth. As shown by equations (12) and (13), the U-shaped and V- shaped are the two types.

$$v = 2 * \cos(2 * \pi * Qe_2) * m \quad (12)$$

$$u = 2 * w(2 * \pi * Qe_3) * n \quad (13)$$

Where, $n = 1 - \frac{md}{mn}$ (14)

In the equation (14), the terms md and mn indicates present iteration and the highest number of iterations. The range of random values is 0 to 1, as in $Qe_2\ and\ Qe_3$. Equation (15) is used to update and determine the new location using these two diving conditions.

$$h_j(m+1) = \begin{cases} h_i(m) + b1 + b2, & 0 \geq 0.5 \\ h_i(m) + a1 + a2, & 0 \geq 0.5 \end{cases} \quad (15)$$

Here, $b2 = v * (h_i$ (m)- $h_i(m) - h_e(m)), and\ a2 = u * (h_i(m) - h_b(n))$ (16)

The terms v and u are represented in equations (16) and (17).

$$v = 2(* Qe_4 - 1) * v, U = (2 * Qe_5 - 1) * u \quad (17)$$

3.5.2.3 Stage 3—Exploitation

It takes considerably more energy to grab the prey once the searchers dash to the water's surface. As a result, as the fish seeks to surface, the gannets may display incredible activity. The following equations (18-21) are used to determine the term D_O.

$$D_O = \frac{1}{o * m2} \quad (18)$$

$$m2 = 1 + \frac{md}{mn} \quad (19)$$

$$o = \frac{nb * uz^2}{K} \quad (20)$$

$$k = 0.2 + (2 - 0.2) * Qc_6 \quad (21)$$

As stated in Qc_6, the random value comes under 0 and 1. Therefore nb and uz represent the gannet's mass and velocity and are set accordingly. Additionally, the equation (22) is used to evaluate the term δ and equation (23) yields the optima value.

$$\delta = do * |h_o(m) h_{as}(m) \quad (22)$$

$$R = kuz(c) \quad (23)$$

3.5.3. Binary Gannet Optimization (BGO) Algorithm

The BGO methodology was expanded upon and altered in this research to handle the unique difficulties of pooling centre placement and transportation optimization. To do this, the new algorithm BGO is proposed and the new mathematical statements are as follows in Equations (24-25)

$$\delta = \frac{\beta}{\gamma}; \gamma = \frac{\beta}{\alpha} \quad (24)$$

The terms α and β in the equation above are calculated as follows:

$$\alpha = \frac{N}{100} \ ; \beta = \frac{N}{20} \quad (25)$$

The total number of populations taken into consideration is indicated by the term N. to get the most effective outcomes, the new gamma values are used in equation (25). Figure 4 represents flow diagram that represents BGO algorithm.

The lung tumor is precisely segmented and classified using an Advanced Computer Vision Model. The integration of BGO-FFNN tends to improve the classification of tumor as normal or abnormal based on the input data. After processing the chosen features from BGO, FFNN discovers trends and connections within the data [34]. This is achieved by BGO that optimizes FFNN hyper parameters. The hyper parameters with its description and values are signified in Table 2. Further, Algorithm 1 represents the steps involved in the proposed model involved in segmentation and classification of lung tumor.

4. Results and Discussion

The outcomes, including comparative analysis and performance evaluation results, are deliberated in this section. Thus, the efficacy of the suggested work is analyzed.

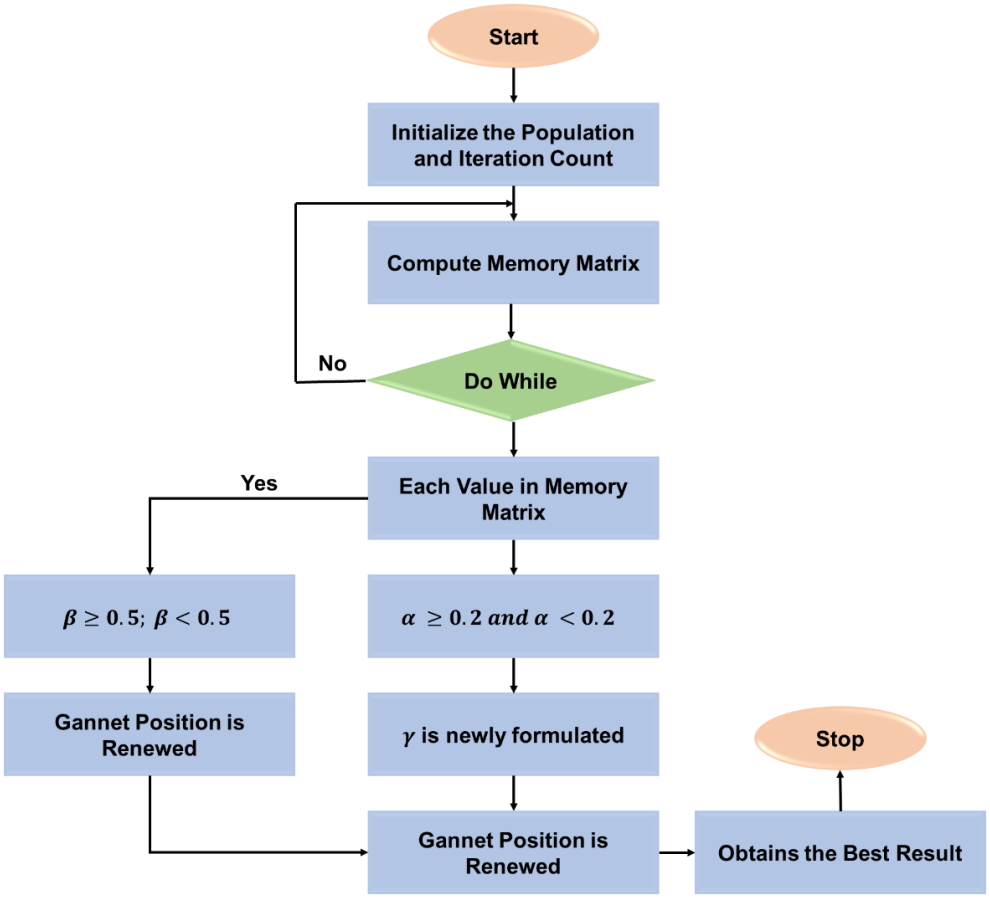

Figure 4. Binary Gannet Optimization (BGO) Algorithm

Table 2. Details of Hyperparameters

Hyperparameter	Description	Values
Number of layers that are hidden.	The FFNN's hidden layer count.	2,3,4
Learning Rate	Speed at which weights are updated by the model during training.	0.001, 0.01, 0.1
Activation Function	The activation function given to each neuron.	Sigmoid, Tanh
Batch Size	Number of samples used in a single training cycle.	16, 32, 64
Epochs	The quantity of thorough runs through the training set.	50, 100, 200

Algorithm 1. Lung Tumor Segmentation and Classification Using MSEWS and BGO-FFNN

Step 1: Tumor Segmentation using MSEWS

```
defmsews 0_segmentation(image):
segmented_image = msews(image)
return segmented_image
segmented_images = []
for image in preprocessed_images:
segmented_image = msews_segmentation(image)
segmented_images.append(segmented_image)
```

Step 2: Feature Extraction using LBP

```
defextract_lbp_features(image):
```

```
lbp_image = local_binary_pattern(image, P=8, R=1, method='uniform')
return lbp_image
lbp_features = []
for image in segmented_images:
features = extract_lbp_features(image)
lbp_features.append(features)
```

Step 3: Initialize FFNN

```
defcreate_ffnn(input_dim, output_dim):
model = tf.keras.Sequential([
tf.keras.layers.Dense(128, activation='relu', input_shape=(input_dim,)),
tf.keras.layers.Dense(64, activation='relu'),
tf.keras.layers.Dense(output_dim, activation='softmax')
return model
```

Step 4: Apply Binary Gannet Optimizer (BGO) to optimize FFNN parameters

```
defbinary_gannet_optimizer(model, features, labels):
bgo = BinaryGannetOptimizer(model, features, labels)
optimized_model = bgo.optimize()
return optimized_model
X = lbp_features
y = dataset.labels
optimized_model = binary_gannet_optimizer(create_ffnn(X.shape[1], len(set(y))), X, y)
```

Step 5: Evaluate Classification Performance

```
model_accuracy = accuracy_score(y_true, y_pred_binary)
model_precision = precision_score(y_true, y_pred_binary)
model_recall = recall_score(y_true, y_pred_binary)
model_f1 = f1_score(y_true, y_pred_binary)
```

4.1 Experimental Setup

The experimental setup to execute the DDEA-NB model needs a high-performance computing system designed and well-fitted with a 1TB SSD, 32 GB RAM, and an Intel Core i9 processor, which can compute large-scale network slicing data efficiently. It is implemented on a Linux-based operating system using Python 3.11.2. The software stack utilizes Scikit-learn for the NB classifier, NumPy and Pandas for data preprocessing, and Matplotlib for visualization.

4.2 Experimental Results

The proposed model BGO-FFNN has been examined, employing several effectiveness criteria, including recall, F1-score, accuracy, as well as precision. These metrics have the descriptions that follow in Table 3. Representing the outcomes procured by the proposed BGO-FFNN model is deliberated in Table 4.

By implementing the proposed model BGO-FFNN, the accuracy obtained is 95.14%, with a precision of 99.71%, recall of 94.48% as well as the F1- score of 97.21%.

4.3. Confusion Matrix

The confusion matrix, which defines true positives and false negatives, assesses the performance of the model. The true tumor type and the false tumor type breakdown enable one to see the positive and negative of the model with respect to their ability to detect and classify tumors. Figure 5 shows the matrix table for the proposed model.

As per the matrix table, 1500 correct instances were obtained as abnormal and 1200 as normal when compared with other misclassified labels.

Table 3. Description of Performance Metrics

Metrics	Explanation	Formula
Accuracy	The capability of the model to predict both true positive and true negatives regarding tumor cases. The model computed an accuracy score, which is the proportion of predictions made that were correct concerning tumor classification, to derive tumor detection and classification results.	$Accuracy = \frac{T_p + T_N}{T_p + T_N + F_P + F_N}$ Where, T_p = True Positives T_N = True Negatives F_P= False Positives F_N=False Negatives
Precision	True Positive-expected ratio relates to the accuracy of tumor instances identified correctly. This parameter measures the ability of the model capable of correctly forecasting positive tumor cases, thus giving an assurance of the reliability of its detection performance.	$Precision = \frac{T_p}{T_p + F_P}$
Recall	The recall is refers to the amount of true positive tumor regions correctly identified among all tumor areas predicted. It emphasizes the model's capability to accurately identify the tumors with higher precision in tumor classification.	$Recall = \frac{T_p}{T_p + F_N}$
F1-score	The F1-score is the tumor classification, harmonic mean of precision and recall: it reflects those points in tumor recognition at which the model has precision (correctly classify the tumors) and recursivity (recognize all of the tumors that it should have done, recall)	$F1 - Score = 2 \times \frac{Precision \times Recall}{Precision + Recall}$

Table 4. Outcomes Produced by Proposed BGO-FFNN

Metrics	BGO-FFNN[Proposed]
Accuracy	95.14
Precision	99.71
Recall	94.48
F1-Score	97.21

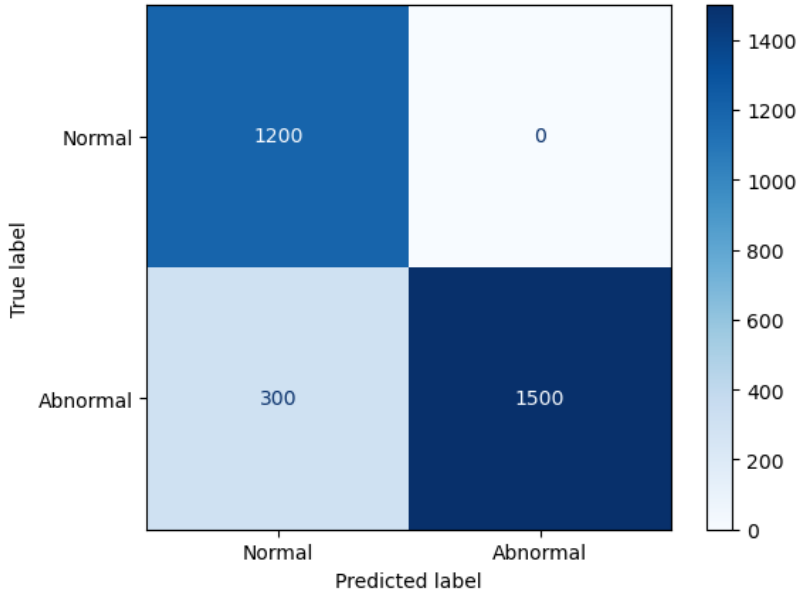

Figure 5. Confusion Matrix

4.4. Receiver Operating Characteristic (ROC)

ROC graph that shows the trade-off between the true positive rate (sensitivity) and the false positive rate, which is used to test the performance of the tumor classifier at various thresholds. This balances the correct identification of tumors and false positives. Figure 6 shows the ROC curve with an AUC of 0.95.

4.5. Comparative Analysis

The BGO-FFNN model is contrasted with other methods to evaluate the efficacy of the developed segmentation as well as the classification model. Conventional models include A Pioneering Educational System Network (APES Net) [28] and Hierarchical Convolutional Neural Network (HCNN) [29, 30]. The comparative results are signified in Table 5 with a graphical illustration in Figure 7.

Tumor detection as well as classification capabilities for APES Net and HCNN are limited. HCNN produces an accuracy of 92.50%, a recall of 91.38%, a precision of 99.63%, and an F1-score of 95.18%, while APESNet attained recall (93.24%), F1-score (96.02%), precision (99.95%), and accuracy (94.32%). These are overcome by the BGO-FFNN model, which achieves improved accuracy (95.14%), recall (94.48%), precision (99.71%), and F1-Score (97.21%). By optimizing the model's parameters, BGO-FFNN enhances the model's performance in tumor segmentation and classification, outperforming existing models.

5. Discussion

For good clinical management, including accurate treatment planning and timely intervention, it is very important to accurately segment and detect lung tumors. Traditional methods often run into big problems, such as the fact that tumor morphology is always changing, the contrast between cancerous and healthy tissues is often subtle, and anatomical structures that overlap can make things even more confusing [35]. These problems always make it harder for traditional methods of tumor delineation and identification to be reliable and accurate. Because of these major flaws, this study presents a new Advanced Computer Vision Model that uses a Binary Gannet Optimizer Tuned Feed Forward Neural Network (BGO-FFNN) to better classify lung tumors.

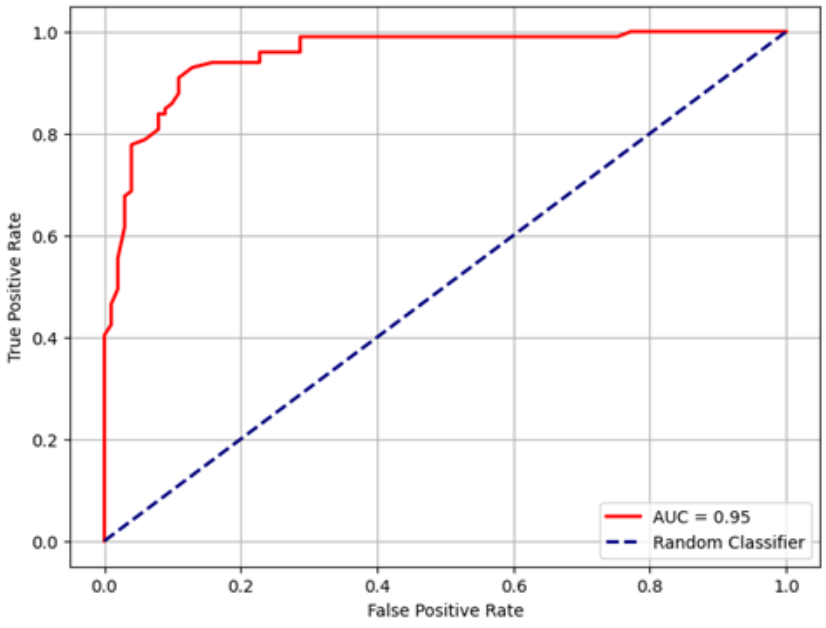

Figure 6. Receiver Operating Characteristic (ROC)

Table 5. Comparative Results for Traditional and Proposed Model

Methods	Accuracy	Precision	Recall	F1-Score
APES Net [29]	94.32	99.95	93.24	96.02
HCNN [29,30]	92.50	99.63	91.38	95.18
BGO-FFNN[Proposed]	95.14	99.71	94.48	97.21

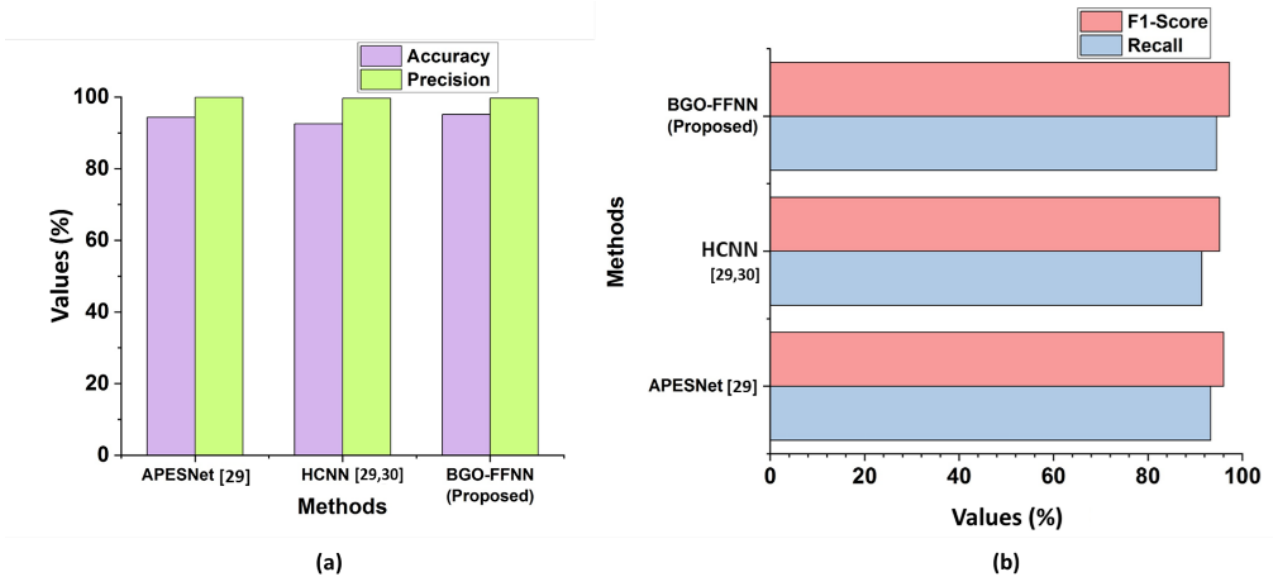

Figure 7. Outcome of the Proposed Model: (a) Accuracy and precision; (b) f1-score and recall

Our proposed method solves the problems listed above with a carefully planned multi-stage process. The first step in preprocessing, which used Gabor filters, worked very well to reduce noise in the images and greatly improve the contrast between tissues. This improvement is very important for making the edges of tumors easier to see, which is necessary for accurate segmentation later on. Using Multi-Scale Edge-Watershed Segmentation (MSEWS) techniques to separate tumor regions showed that they could do so with a high level of accuracy [36]. This hybrid method works well because it combines edge detection with watershed principles. This lets it capture complex tumor shapes that other single-strategy methods might miss. Also, using Local Binary Patterns (LBP) to get texture features gave the model useful detailed textural information that helped it tell different types of tumors apart based on their unique micro-architectural features.

The main new thing about this work is that it uses the Binary Gannet Optimizer (BGO) to make the Feed Forward Neural Network (FFNN) work better. This meta-heuristic optimization method worked well to fine-tune the FFNN's parameters, which improved its ability to classify. The experimental results clearly show that the proposed BGO-FFNN model works, with impressive metrics across all evaluated parameters: recall (94.48%), F1-score (97.21%), accuracy (95.14%), and precision (99.71%). These numbers show that the model can accurately find positive cases (high recall), keep a good balance between precision and recall (high F1-score), correctly label both tumor and non-tumor areas (high accuracy), and keep false positives to a minimum (high precision).

When we compare our results to those of traditional methods, we see that the suggested advanced computer vision model performs much better. With powerful adaptation capabilities of BGO for FFNN architecture, advanced image processing techniques (Gabor filtering, msws), strong convenience extraction (LBP) [37], and with co -integral integration of the powerful adaptation abilities of BGO for FFNN architecture, make it better. The fact that this hybrid model can achieve around problems with traditional methods shows how it can change the way the lung tumor is seen.

This study has a major impact on how it can be used in the clinic. The BGO-FFNN model can help radiologist and pathologist to get more accurate tumor assessment and diagnose by creating a very easy to find and classify the tumor. This high accuracy can directly make better treatment plans, allowing better patient results and less mistakes in diagnosis [38]. In the future, we will work on testing the model on large and more diverse datasets, given whether it can be used with a variety of imaging, and to see how it can be used in real -time clinical workflows.

We used two separate existing methods, APESNet [39] and HCNN [40], to see how well the proposed model worked. However, a low recall rate of APESNet suggests that the tumor can be miscarried. Also, HCNN with low accuracy values tends to make classification less reliable. But these problems can be fixed by using the suggested BGO-FFNN model, which gets rid of unnecessary and unimportant features. This makes the model work better and lowers its dimensionality. The BGO-FFNN model works better than APES Net and HCNN because it has better recall, can automatically change hyper parameters, chooses the best features, and is more accurate. Because of these improvements, the tumor segmentation and classification model is now more effective and reliable.

6. Conclusion

This study successfully created and tested a new advanced computer vision model to classify the lung tumors. It used a binary gennet optimizer tune feed forward neural network (BGO-FFNN). Our model showed a strong and accurate way to find and separate the lung tumors, even if traditional methods have their own problems. The suggested method uses a gabber filter to reduce the noise and vice versa, correctly tumor to multi-level edge-watarashed segmentation (MSEWP), and important texture features for local binary pattern (LBP) (LBP) (LBP). There was a major difference in classification from using a binary gennet optimizer in a new way to improve the performance of feedform neural networks.

This study uses an advanced computer vision model to block and classify the lung tumors. First, input data were collected, including images from histopathology and radiology. Then, the Gabor filter was used to get rid of noise, MSEWS was used to separate the tumor, and LBP was used to achieve text features from different input images. After that, BGO optimizes FFNN hyper parameters to classify images as normal or unusual. Results suggest that proposed model tumor classification and detection is better than existing methods, accuracy of 95.14%, accuracy of 99.71%, a recall of 94.48%, and F1-score of 97.21%. This improvement increases the tumor segment and classification efficiency. Infrastructure can also be biased of training data even after adaptation, especially when working with small or unbalanced datasets. This hybrid model represents a significant progress in the field of medical image analysis, which provides sufficient improvement in tumor detection and classification accuracy. The potential clinical effect is deep, as this model can serve as an invaluable tool to support radiologists and pathologists and assess and diagnose more accurate and timely. By contributing to the more accurate treatment plan and early intervention, the BGO-FFNN model promises greatly to improve patient results in lung cancer management. To increase generalization, future research should focus on data growth approach and large, more diverse datasets.

References

[1] A. Shimazaki, D. Ueda, A. Choppin, A. Yamamoto, T. Honjo, Y. Shimahara, Y. Miki, Deep learning-based algorithm for lung cancer detection on chest radiographs using the segmentation method. Scientific Reports, 12(1), (2022) 727. https://doi.org/10.1038/s41598-021-04667-w

[2] S.P. Primakov, A. Ibrahim, J.E. van Timmeren, G. Wu, S.A. Keek, M. Beuque, R.W. Granzier, E. Lavrova, M. Scrivener, S. Sanduleanu, E. Kayan, Automated detection and segmentation of non-small cell lung cancer computed tomography images. Nature Communications, 13(1), (2022) 3423. https://doi.org/10.1038/s41467-022-30841-3

[3] O. Akter, M.A. Moni, M.M. Islam, J.M. Quinn, A.H.M. Kamal, Lung cancer detection using enhanced segmentation accuracy. Applied Intelligence, 51, (2021) 3391-3404. https://doi.org/10.1007/s10489-020-02046-y

[4] R. Mahum, A.S. Al-Salman, Lung-RetinaNet: Lung cancer detection using a RetinaNet with multi-scale feature fusion and context module. IEEE Access, 11, (2023) 53850-53861. https://doi.org/10.1109/ACCESS.2023.3281259

[5] I. Nazir, I.U. Haq, M.M. Khan, M.B. Qureshi, H. Ullah, S. Butt, Efficient pre-processing and segmentation for lung cancer detection using fused CT images. Electronics, 11(1), (2021) 34. https://doi.org/10.3390/electronics11010034

[6] K.V. Rani, S.J. Jawhar, Novel technology for lung tumor detection using nanoimage. IETE Journal of Research, 67(5), (2021) 699-713. https://doi.org/10.1080/03772063.2019.1565955

[7] P. Dutande, U. Baid, S. Talbar, Deep residual separable convolutional neural network for lung tumor segmentation. Computers in Biology and Medicine, 141, (2022) 105161. https://doi.org/10.1016/j.compbiomed.2021.105161

[8] J. Chamberlin, M.R. Kocher, J. Waltz, M. Snoddy, N.F. Stringer, J. Stephenson, P. Sahbaee, P. Sharma, S. Rapaka, U.J. Schoepf, A.F. Abadia, J. Sperl, P. Hoelzer, M. Mercer, N. Somayaji, G. Aquino, J.R. Burt, Automated detection of lung nodules and coronary artery calcium using artificial intelligence on low-dose CT scans for lung cancer screening: accuracy and prognostic value. BMC Medicine, 19, (2021) 1-14. https://doi.org/10.1186/s12916-021-01928-3

[9] R.R. Savjani, M. Lauria, S. Bose, J. Deng, Y. Yuan, V. Andrearczyk, Automated tumor segmentation in radiotherapy. Seminars in Radiation Oncology, 32(4), (2022) 319-329. https://doi.org/10.1016/j.semradonc.2022.06.002

[10] S. Avinash, H.N. Naveen Kumar, M.S. Guru Prasad, R. Mohan Naik, G. Parveen, Early detection of malignant tumor in lungs using feed-forward neural network and K-nearest neighbor classifier. SN Computer Science, 4(2), (2023) 195. https://doi.org/10.1007/s42979-022-01606-y

[11] C. Venkatesh, P. Bojja, A dynamic optimization and deep learning technique for detection of lung cancer in CT images and data access through Internet of Things. Wireless Personal Communications, 125(3), (2022) 2621–2646. https://doi.org/10.1007/s11277-022-09676-0

[12] M.D. Javeed, R. Nagaraju, R. Chandrasekaran, G. Rajulu, P. Tumuluru, M. Ramesh, S.K. Suman,

R. Shrivastava, Brain tumor segmentation and classification with hybrid clustering, probabilistic neural networks. Journal of Intelligent & Fuzzy Systems, 45(4), (2023) 6485-6500. https://doi.org/10.3233/JIFS-232493

[13] G. Geethu Lakshmi, P. Nagaraj, (2025) Lung cancer detection and classification using optimized CNN features and Squeeze-Inception-ResNeXt model. Computational Biology and Chemistry, 117, 108437. https://doi.org/10.1016/j.compbiolchem.2025.108437

[14] H. Liz-Lopez, A.A. de Sojo-Hernández, S. D'Antonio-Maceiras, M.A. Diaz-Martinez, D. Camacho, Deep learning innovations in the detection of lung cancer: Advances, trends, and open challenges. Cognitive Computation, 17(2), (2025) 67. https://doi.org/10.1007/s12559-025-10408-2

[15] M. Alavinejad, M. Shirzad, M.J. Javid-Naderi, A. Rahdar, S. Fathi-Karkan, S. Pandey, Smart nanomedicines powered by artificial intelligence: a breakthrough in lung cancer diagnosis and treatment. Medical Oncology, 42(5), (2025) 134. https://doi.org/10.1007/s12032-025-02680-x

[16] D. Xiang, B. Zhang, Y. Lu, S. Deng, Modality-specific segmentation network for lung tumor segmentation in PET-CT images. IEEE Journal of Biomedical and Health Informatics, 27(3), (2022) 1237–1248. https://doi.org/10.1109/JBHI.2022.3186275

[17] X. Fu, L. Bi, A. Kumar, M. Fulham, J. Kim, Multimodal spatial attention module for targeting multimodal PET-CT lung tumor segmentation. IEEE Journal of Biomedical and Health Informatics, 25(9), (2021) 3507–3516. https://doi.org/10.1109/JBHI.2021.3059453

[18] J. Yang, B. Wu, L. Li, P. Cao, O. Zaiane, MSDS-UNet: A multi-scale deeply supervised 3D U-Net for automatic segmentation of lung tumor in CT. Computerized Medical Imaging and Graphics, 92, (2021) 101957. https://doi.org/10.1016/j.compmedimag.2021.101957

[19] P. Princy Magdaline, T.R. Ganesh Babu, R. Praveena, R. Khowshalya, A Hybrid Deep Learning Model Combining AgresNet, YOLO, and CNN for Lung Tumor Segmentation and Classification. Journal of Innovative Image Processing, 6(4), (2025) 472–498. https://doi.org/10.36548/jiip.2024.4.009

[20] V.R. Nitha, S.S.V. Chandra, ExtRanFS: An automated lung cancer malignancy detection system using extremely randomized feature selector. Diagnostics, 13(13), (2023) 2206. https://doi.org/10.3390/diagnostics13132206

[21] H.T. Gayap, M.A. Akhloufi, Deep machine learning for medical diagnosis, application to lung cancer detection: a review. Biomed Informatics, 4(1), (2024) 236–284. https://doi.org/10.3390/biomedinformatics4010015

[22] M. Kashyap, X. Wang, N.Panjwani, M. Hasan, Q. Zhang, C. Huang, K. Bush, A. Chin, L.K. Vitzthum, P. Dong, S. Zaky, Automated Deep Learning-Based Detection and Segmentation of Lung Tumors at CT. Radiology, 314(1), (2025) e233029. https://doi.org/10.1148/radiol.233029

[23] S. Vijh, P. Gaurav, H.M. Pandey, Hybrid bio-inspired algorithm and convolutional neural network for automatic lung tumor detection. Neural Computing and Applications, 35(33), (2023) 23711–23724. https://doi.org/10.1007/s00521-020-05362-z

[24] S. Momin, Y. Lei, Z. Tian, T. Wang, J. Roper, A.H. Kesarwala, K. Higgins, J.D. Bradley, T. Liu, X. Yang, Lung tumor segmentation in 4D CT images using motion convolutional neural networks. Medical Physics, 48(11), (2021) 7141–7153. https://doi.org/10.1002/mp.15204

[25] R. Raza, F. Zulfiqar, M.O. Khan, M. Arif, A. Alvi, M.A. Iftikhar, T. Alam, Lung-EffNet: Lung cancer classification using EfficientNet from CT-scan images. Engineering Applications of Artificial Intelligence, 126, (2023).106902. https://doi.org/10.1016/j.engappai.2023.106902

[26] Tian, Q., Wu, Y., Ren, X. and Razmjooy, N. (2021). A new optimized sequential method for lung tumor diagnosis based on deep learning and converged search and rescue algorithm. Biomedical Signal Processing and Control, 68, p.102761. https://doi.org/10.1016/j.bspc.2021.102761

[27] T. Meraj, H.T. Rauf, S. Zahoor, A. Hassan, M.I. Lali, L. Ali, S.A.C. Bukhari, U. Shoaib, Lung nodules detection using semantic segmentation and classification with optimal features. Neural Computing and Applications, 33, (2021) 10737–10750. https://doi.org/10.1007/s00521-020-04870-2

[28] J. Soltani-Nabipour, A. Khorshidi, B. Noorian, Lung tumor segmentation using improved region growing algorithm. Nuclear Engineering and Technology, 52(10), (2020) 2313–2319. https://doi.org/10.1016/j.net.2020.03.011

[29] P.K.F. Chiu, X. Shen, G. Wang, C.L. Ho, C.H. Leung, C.F. Ng, K.S. Choi, J.Y.C. Teoh, Enhancement of prostate cancer diagnosis by machine learning techniques: an algorithm development and validation study. Prostate Cancer and Prostatic Diseases, 25(4), (2022) 672–676. https://doi.org/10.1038/s41391-021-00429-x

[30] P.K. Balasubramanian, W.C. Lai, G.H. Seng, J. Selvaraj, Apestnet with mask R-CNN for liver tumor segmentation and classification. Cancers, 15(2), (2023) 330. https://doi.org/10.3390/cancers15020330

[31] S. Saha Roy, S. Roy, P. Mukherjee, A. Halder Roy, An automated liver tumour segmentation and classification model by deep learning-based approaches. Computer Methods in Biomechanics and Biomedical Engineering: Imaging & Visualization, 11(3), (2023) 638-650. https://doi.org/10.1080/21681163.2022.2099300

[32] Y. Akbari, F. Abdullakutty, S. Al Maadeed, A. Bouridane, R. Hamoudi, Breast cancer detection based on histological images using fusion of diffusion model outputs. Scientific Reports, 15(1), (2025) 21463. https://doi.org/10.1038/s41598-025-05744-0

[33] R. Pradeep Kumar Reddy, R. Lakshmi Pravallika, A spatially constrained density-weighted clustering method for brain tumor segmentation in MRI images. International Research Journal of Multidisciplinary Technovation, 7(3), (2025) 345–364. https://doi.org/10.54392/irjmt25325

[34] A. Raza, A. Guzzo, M. Ianni, R. Lappano, A. Zanolini, M. Maggiolini, G. Fortino, Federated learning in radiomics: A comprehensive meta-survey on medical image analysis. Computer Methods and Programs in Biomedicine, 267, (2025) 108768. https://doi.org/10.1016/j.cmpb.2025.108768

[35] M. Shekhar, S. Khetavath, Implementing lung cancer diagnosis framework in early stages using segmentation procedures and adaptive recurrent convolution neural network with region attention for classification. Sensing and Imaging, 26(43), (2025) 1–38. https://doi.org/10.1007/s11220-025-00572-y

[36] K.V. Aishwarya, A. Asuntha, A survey on comparative study of lung nodules applying machine learning and deep learning techniques. Multimedia Tools and Applications, 84(5), (2025) 2127–2181. https://doi.org/10.1007/s11042-024-20009-0

[37] M. Pallumeera, J.C. Giang, R. Singh, N.S. Pracha, M.S. Makary, Evolving and novel applications of artificial intelligence in cancer imaging. Cancers, 17(9), (2025) 1510. https://doi.org/10.3390/cancers17091510

[38] S.C. Kotoulas, D. Spyratos, K. Porpodis, K. Domvri, A. Boutou, Kaimakamis, E. C. Mouratidou, V. Dourliou, K.Tsakiri, A. Sakkou, A. Marneri, E. Angeloudi, I. Papagiouvanni, A. Michailidou, K. Malandris, K.C. Mourelatos, A. Tsantos, A. Pataka, A thorough review of the clinical applications of artificial intelligence in lung cancer. Cancers, 17(5), (2025) 882. https://doi.org/10.3390/cancers17050882

[39] S.U. Aswathy, P.P. Fathimathul Rajeena, A. Abraham, D. Stephen, Deep learning-based BoVW–CRNN model for lung tumor detection in nano-segmented CT images. Electronics, 12(1), (2022) 14. https://doi.org/10.3390/electronics12010014

[40] I. Naseer, S. Akram, T. Masood, M. Rashid, A. Jaffar, Lung cancer classification using modified U-Net based lobe segmentation and nodule detection. IEEE Access, 11, (2023) 60279–60291. https://doi.org/10.1109/ACCESS.2023.3285821

Authors Contribution Statement

Both the authors equally contributed, read and approved the final version of this manuscript.

Funding

The authors declare that no funds, grants or any other support were received during the preparation of this manuscript.

Competing Interests

The authors declare that there are no conflicts of interest regarding the publication of this manuscript.

Data Availability

The data supporting the findings of this study can be obtained from the corresponding author upon reasonable request.

Has this article screened for similarity?

Yes

About the License